

RECEIVED: March 13, 2017

REVISED: May 18, 2017

ACCEPTED: June 12, 2017

PUBLISHED: June 27, 2017

P-Type Silicon Strip Sensors for the new CMS Tracker at HL-LHC



The Tracker Group of the CMS Collaboration

E-mail: alexander.dierlamm@kit.edu

ABSTRACT: The upgrade of the LHC to the High-Luminosity LHC (HL-LHC) is expected to increase the LHC design luminosity by an order of magnitude. This will require silicon tracking detectors with a significantly higher radiation hardness. The CMS Tracker Collaboration has conducted an irradiation and measurement campaign to identify suitable silicon sensor materials and strip designs for the future outer tracker at the CMS experiment. Based on these results, the collaboration has chosen to use n-in-p type silicon sensors and focus further investigations on the optimization of that sensor type.

This paper describes the main measurement results and conclusions that motivated this decision.

KEYWORDS: Particle tracking detectors (Solid-state detectors); Radiation-hard detectors; Detector modelling and simulations II (electric fields, charge transport, multiplication and induction, pulse formation, electron emission, etc)

Corresponding author: Alexander Dierlamm.

Contents

1	Introduction	1
2	Samples and irradiations	2
3	Initial characterization	5
3.1	Electrical characterization	5
3.2	Charge collection and noise	5
4	Performance after irradiation	6
4.1	Electrical characterization	6
4.2	Charge collection and noise	9
5	Simulation of electric fields	14
6	Conclusion	16
	Tracker group of the CMS collaboration	20

1 Introduction

The LHC is foreseen to be upgraded to the High-Luminosity LHC (HL-LHC), which will provide an instantaneous luminosity of up to $5\text{--}7.5 \cdot 10^{34} \text{ cm}^{-2}\text{s}^{-1}$ for an integrated luminosity of 3000 fb^{-1} [1, 2] (up to 4000 fb^{-1} , if the ultimate instantaneous luminosity can be achieved). This increase in luminosity will require silicon trackers with a significantly higher granularity and radiation hardness compared to the existing ones [3]. The current CMS Tracker consists of 200 m^2 of p-in-n type (p-type strip implants in n-type bulk) silicon strip sensors. The strip pitches range from $80 \mu\text{m}$ to $205 \mu\text{m}$, the strip lengths from 10 cm to 20 cm and the maximum expected fluence is $1.8 \times 10^{14} \text{ n}_{\text{eq}}/\text{cm}^2$ [4]. The future CMS outer tracker will extend from a radius of 20 cm to 110 cm around the beam pipe. It will utilize silicon strip sensors with $90 \mu\text{m}$ pitch and a strip length of 5 cm (at radii larger than 60 cm) and for the inner region (at radii between 20 cm and 60 cm) a similar strip sensor with $100 \mu\text{m}$ pitch and a strip length of 2.5 cm as well as a macro-pixel sensors with a pitch of $100 \mu\text{m}$ and a pixel length of 1.5 mm . The macro-pixels in the inner layers are motivated by the requirement for higher granularity and better pointing resolution in the Z-direction (along the beam pipe) for standalone tracks in the outer tracker. The total active silicon area will sum up to about 190 m^2 . As illustrated in figure 1, the fluence equivalent to the damage caused by 1 MeV neutrons is estimated to reach about $1.1 \times 10^{15} \text{ n}_{\text{eq}}/\text{cm}^2$ at the inner radius of the outer tracker (corresponding to 3000 fb^{-1}). The expected total ionizing dose ranges from 10 kGy to 750 kGy [3]. The range of particles that the detectors will be exposed to consists of charged particles and neutral particles with a ratio of 1:1 in the inner region up to 1:10 in the outer region. It was already shown in [6] that defect

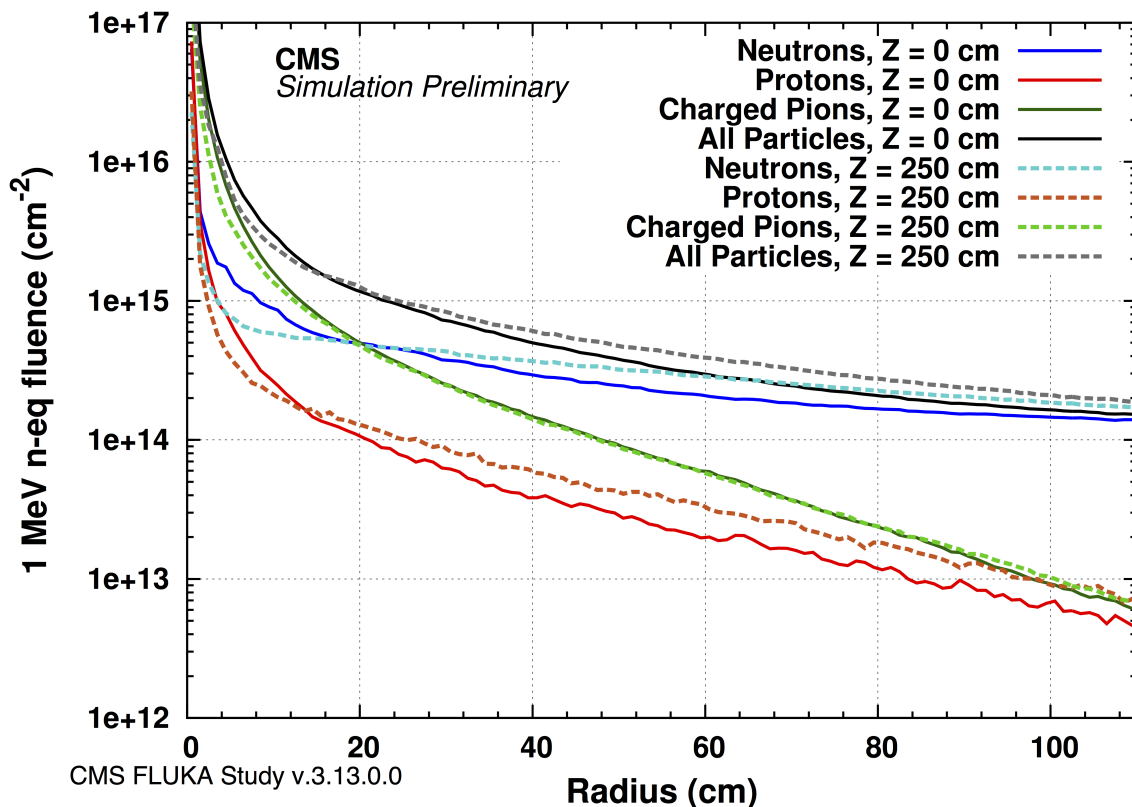


Figure 1. FLUKA simulation of the fluence levels in the CMS Tracker after 3000 fb^{-1} [5]. The Z-coordinate in the legend refers to the distance from the interaction point along the beam line.

formation in silicon depends on the particle type and energy. In addition, ionizing radiation due to charged particles increases the oxide charge density of the silicon dioxide [7–10], which affects the surface properties of the strip sensors. Therefore, an irradiation and measurement campaign including (mixed) irradiations with both neutrons and protons (both low and high energy protons were used) was performed, for which results have been published in PhD theses and conference reports [11–21]. A general description of the campaign, the used materials, results from diode measurements (IV, CV, TCT), strip sensor characterizations and annealing studies will be reported in a future publication.

This paper presents results derived from measurements using small prototype strip sensors (table 1), including those that illustrate the performance of irradiated p-in-n and n-in-p sensor types, and motivates the conclusion that n-in-p type sensors are most appropriate for use in the CMS Tracker Phase II Upgrade. The results referred to in this paper are described in several of the aforementioned publications and therefore only the most relevant ones, on which the decision is based on, are summarized for the first time.

2 Samples and irradiations

The AC coupled strip sensors used in this study were processed by one single vendor (Hamamatsu Photonics K.K. (HPK)) on several wafer types with the same mask set. This approach allowed

Table 1. Layout and process details of the two studied miniature strip sensors. Due to space limitations the strip lengths are not the same as for the final design.

Parameter	Value
Strip length	3.27/2.57 cm
Strip width	19 μm
Strip pitch	80 μm
Strip metal width	31 μm
No. of strips	256 / 64
No. of guard rings	1
Overall dimensions	3.5 cm \times 2.3 cm / 2.8 cm \times 1.3 cm
Coupling dielectric thickness	300 nm ($\text{SiO}_2/\text{Si}_3\text{N}_4$)
Strip doping conc. (peak)	$\sim 1 \times 10^{19} \text{ cm}^{-3}$
p-stop doping conc. (peak)	$\sim 5 \times 10^{15} \text{ cm}^{-3}$
p-spray doping conc. (peak)	$\sim 1 \times 10^{15} \text{ cm}^{-3}$

a direct comparison of the properties of the base materials without the additional influence of manufacturing techniques and quality levels employed by different vendors. The details of the sensor layouts are listed in table 1. The sensor types discussed in this paper are n-in-p (highly n-doped strips in p-doped bulk) sensors with p-stop or p-spray strip isolation as well as p-in-n sensors [22]. Sensors of n-in-n type have not been considered as the associated costs are expected to be much higher and the required double-sided process is more prone to damage of the sensitive backside. The charge collection is expected to be equal to the charge collection of n-in-p type sensors, since the same charge carriers are collected. The sensors are processed on wafers of different thicknesses: thinned wafers made from float-zone silicon (FZ) with a physical and active thickness of 200 μm and deep-diffused FZ wafers (ddFZ) [23] with a physical thickness of 320 μm and a nominal active thickness of 300 μm or 200 μm . The active thickness (low doping concentration) for these ddFZ wafers is reduced from the physical thickness of 320 μm by a long-term thermal treatment allowing the high backside doping to diffuse deep into the bulk. One reason for using 200 μm thin sensors is to reduce the material of the tracker (less conversions and multiple-scattering). In addition, thin sensors have a higher average electric field at the maximum operation voltage of 600 V compared to thicker sensors and therefore reduce the drift time (and trapping probability after irradiation). The resistivity of the base material is greater than 3 k Ω cm leading to an initial full depletion voltage below 300 V.

After initial characterization, the sensors were first exposed to reactor neutron irradiations or proton irradiations and in a second step irradiation with the other particle type was carried out resulting in a mixed irradiation scenario (according to table 2). The fluences were chosen such that the mixed fluences represent approximately the situation at the innermost radii for the two sensor types plus a safety factor of 30% ($7 \times 10^{14} \text{ n}_{\text{eq}}/\text{cm}^2$ for strip sensors at 60 cm and $1.5 \times 10^{15} \text{ n}_{\text{eq}}/\text{cm}^2$ for macro-pixel sensors at 20 cm). The fluences for individual particles were selected in such a way that one could interpolate the behavior for protons and neutrons independently and then also compare the two. The selection was limited by the number of available samples and time constraints. For most of the materials and fluence points one sensor was measured.

Table 2. Overview of irradiations. The listed values approximate the expected conditions in the detector during operation. Samples are measured after irradiation with one particle type, and after irradiation with the other particle type measurements for several annealing durations follow. Higher mixed fluence represents a location closer to the interaction point, where charged particles dominate. A fluence of 1.5×10^{15} n_{eq}/cm^2 corresponds to a radius in the tracker of about 20 cm (innermost radius) and 7×10^{14} n_{eq}/cm^2 to 60 cm (transition between macro-pixel and strip sensor modules) after 3000 fb^{-1} plus safety factor of about 30 %.

Total Fluence / $10^{14} \text{ } n_{eq}/\text{cm}^2$	Proton fraction	Neutron fraction
3	1	0
4	0	1
5	0	1
7	0.43	0.57
10	1	0
10	0	1
15	0.67	0.33
15	1	0

Although the particle type with the highest flux in the CMS tracker are charged pions of about 500 MeV [24, 25] this particle type is not easily available for irradiation tests. The particle type with displacement damage very similar to these pions are high energy protons [26], which were considered as the reference particle type for charged hadron damage in this study. Low energy protons are used for comparison and to extend the amount of test points, since they are most easily accessible.

The samples were characterized after the first irradiation step and a short annealing of about 10 minutes at 60°C (equivalent to approximately two days at 20°C according to the scaling of the leakage current as given by [27]) to equalize different annealing conditions during irradiation and transport. After the second irradiation the samples were characterized after each of several consecutive annealing steps in order to study the change of properties with time at room temperature. This information can be used to define the temperature during maintenance periods and possibly exploit beneficial changes at room temperature.

In addition, low (23 MeV) and high (24 GeV) energy protons were used to study the influence on defect generation [18]. No significant difference in charge collection (see section 4.2) and noise was observed.

The neutron irradiation was performed at the TRIGA Mark II reactor [28] at Josef-Stefan-Institute, Ljubljana, Slovenia. The fluences were reached within 5 minutes¹ at about 40°C followed by a 30 minutes period at 30°C in the irradiation channel for deactivation. The GeV proton irradiation at the proton synchrotron (PS) [30], CERN, Switzerland, took one to three days at 25°C . The MeV proton irradiation at the Karlsruhe Compact Cyclotron (KAZ) [31], ZAG, Germany, took less than an hour at around -30°C . All samples were stored in a freezer below -5°C after irradiation to prevent further annealing.

¹Earlier studies have shown that this high flux does not change the irradiation effects [29].

3 Initial characterization

After production and dicing, the samples were characterized before irradiation in terms of static electrical sensor parameters, charge collection and noise performance.

3.1 Electrical characterization

Initially, all sensors were electrically characterized in a probe station. The following measurements were performed:

Total leakage current. The current on the bias line is measured versus bias voltage (IV) with floating guard ring. Good sensors shall not exceed 2 nA/mm^3 .

Total capacitance. The capacitance of the sensor is measured versus bias voltage (IV) with floating guard ring to extract the full depletion voltage.

Strip leakage currents. The leakage current of individual strips are measured to check the uniformity.

Coupling capacitance. The capacitance between strip implant and metal strip is measured at 100 Hz. The capacitance shall be larger than $1.2 \text{ pF}/(\text{cm} \times \mu\text{m})$.

Current through the dielectric. The current is measured between strip implant and metal strip applying 10 V. The current shall be smaller than 1 nA.

Bias resistance. The bias resistor at each strip is evaluated by measuring the current when applying 2 V on the DC pad. A resistance between 1.2 and 1.8 M Ω is envisaged.

Interstrip capacitance. The capacitance between neighboring metal strips is measured at 1 MHz and should be below 1 pF/cm.

Interstrip resistance. The resistance between two strip implants is evaluated by measuring the IV characteristic from -1 V to 1 V . The resistance should be about ten times higher than the bias resistance; before irradiation even larger than 10 G $\Omega \text{ cm}$.

An overview of these results can be found in [32]. Within these initial measurements no significant difference in the properties of n-in-p and p-in-n sensors was observed.

3.2 Charge collection and noise

The charge collection and the noise of the sensors were measured using the ALiBaVa system [33] based on the Beetle chip [34] and a Sr-90 source. A picture of such a setup is shown in figure 2. The noise is defined as the RMS of the signal per channel taken with random triggers. Internal calibration pulses provide the gain to translate ADC counts into charge in electrons with an uncertainty of about 10% [35]. A noise of 900 e^- per channel is measured with the Beetle chip for these sensors. This noise figure is in the order of magnitude expected for a system operated with the CBC read-out chip [36] developed for the future CMS strip sensor modules. The noise measured here does not exactly reflect the noise of the final modules in the upgraded CMS tracker, but still relative noise changes can be used to characterize the impact of different layouts or irradiation levels.

For charge collection measurements, the data acquisition is triggered by a scintillator plus photomultiplier tube placed below the sensor. Clusters are identified by finding channels (see

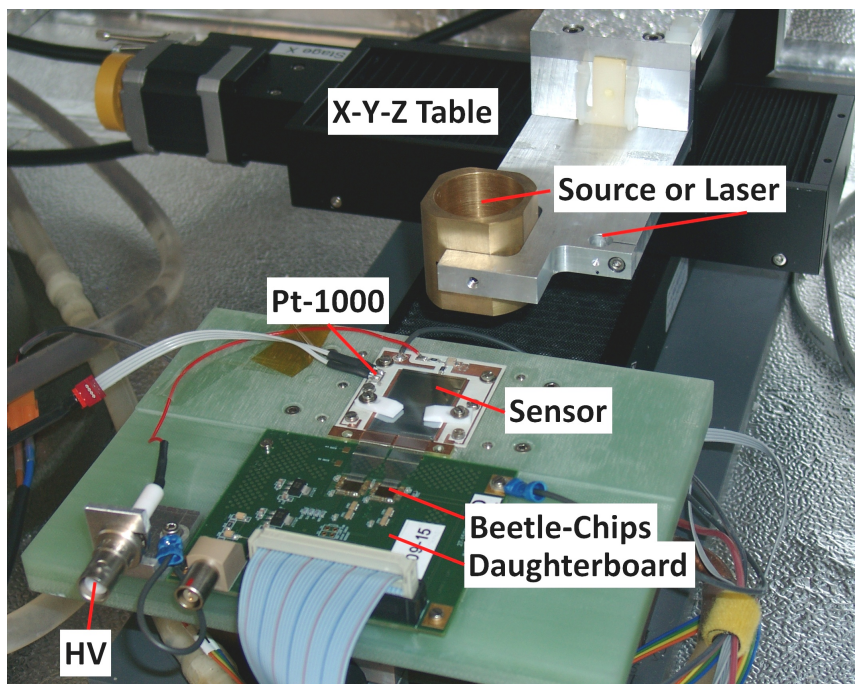


Figure 2. The measurement setup at KIT based on the ALiBaVa system.

strips) with a signal that exceeds five times their noise. Then, neighboring channels with a signal above two times their noise are associated with the same cluster. An example of the cluster charge distribution is given in figure 3. The most probable value (MPV) of the convoluted Landau-Gauss fit is at $15\,700\,e^-$, which translates to $74.8\,e^-/\mu\text{m}$ given the active thickness of about $210\,\mu\text{m}$ for this sensor type as derived from CV measurements. The usage of a Sr-90 source together with one scintillator adds a minor fraction of low energetic electrons to the spectrum increasing the average deposited energy by only about 2%. Within the stated uncertainty of the calibration pulse this measurement is still compatible with about $75.3\,e^-/\mu\text{m}$ as expected from [37] for $\beta\gamma > 100$. For $300\,\mu\text{m}$ thick sensors a cluster charge of $22\,500\,e^-$ is expected.

The charge collection study is focused on evaluating the seed signal only, since the CBC works in binary mode. The analog input signal will be fed into a programmable comparator for each individual channel without any clustering algorithm. Therefore the single strip charge (here that means the seed signal) has to exceed the threshold set in the readout chip for full efficiency. The average cluster width is about 1.5 to 2 strips and the seed signal is about 80% to 90% of the cluster signal before irradiation.

4 Performance after irradiation

4.1 Electrical characterization

After irradiation the sensors were again characterized electrically in probe stations at $-20\,^\circ\text{C}$, which is the approximate temperature during operation in the CMS detector. Strip parameters, IV and CV measurements are presented in [32]. The full depletion voltages and the volume generated

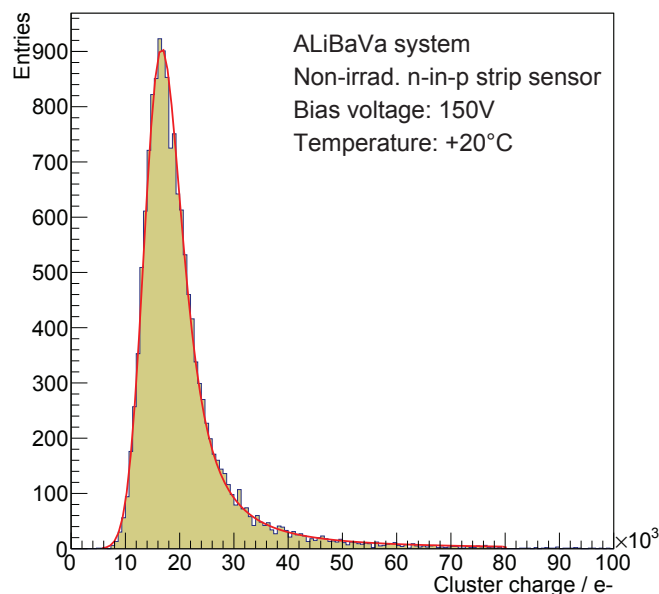


Figure 3. Cluster charge distribution for a non-irradiated n-in-p type sensor with 210 μm active thickness at 150 V bias voltage and a temperature of 20 $^{\circ}\text{C}$. The red line is a convoluted Landau-Gauss fit. The data were acquired with an ALiBaVa system as described in the text.

currents are reproduced in figures 4 and 5. Except for the expected increase in leakage currents (total as well as for individual strips), the expected tendency of increasing full depletion voltage after possible type inversion and a reduction of the interstrip resistance, no significant changes were observed. Most notably, the interstrip capacitance, which is a big contribution to the noise, did not change much as shown in figure 6. Looking at the post-irradiation data one can see a tendency that the values for n-in-p type sensors are slightly higher, but still within the errors, which could lead to a small noise increase of up to 3%. The interstrip resistance² dropped from larger than 1 T Ω cm to between 1 G Ω cm and 10 G Ω cm (figure 7). For correct operation of the sensors, the interstrip resistance should be at least 10 times larger than the resistance of the bias resistors (~ 2 M Ω). That would require an interstrip resistance of 20 M Ω . The final sensors will have 5 cm long strips. As test criterion for sensors of different length a minimum of 100 M Ω cm is required. On average this value is exceeded by a large margin with even the lowest measurements lying above this value. Figure 7 also shows that there is no significant difference between the isolation techniques. Both p-stop and p-spray techniques as processed by HPK fulfill the requirements. This means that it is possible to produce n-in-p sensors with sufficient strip isolation which can withstand fluences of up to 1.5×10^{15} n_{eq}/cm², using either isolation technique. This is also demonstrated by simulations in [38]. It should be pointed out that a careful selection of process parameters is necessary to ensure the interstrip resistances demonstrated by the samples. A very low p-stop concentration leads to a low interstrip resistance and therefore to a short-circuit of the strips resulting in large

²Here the resistance was normalized to the strip length. Longer strips result in lower resistance values.

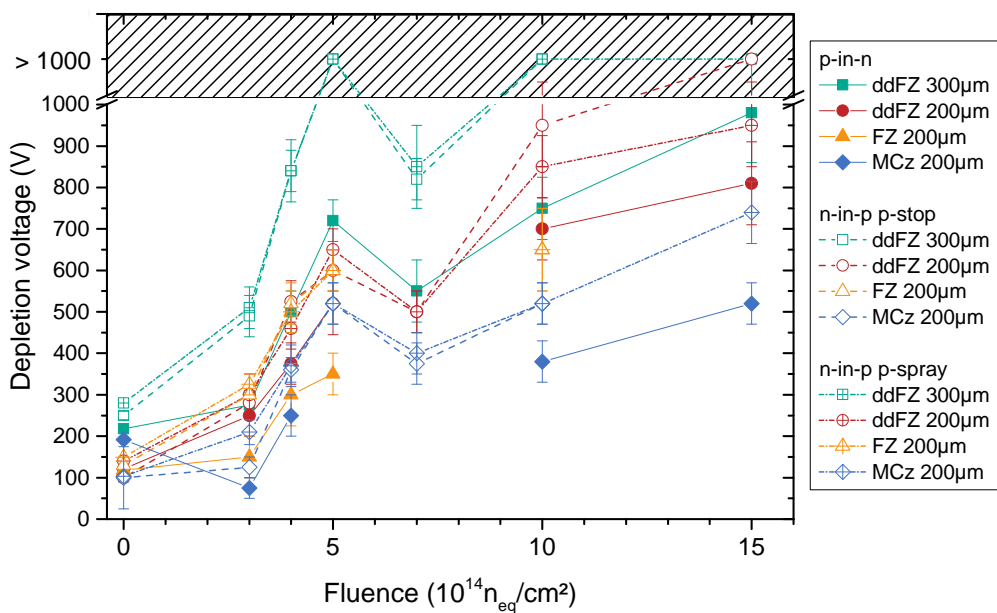


Figure 4. Full depletion voltages of strip sensors as extracted from CV measurements [32]. Measurements on non-irradiated samples were performed at room temperature, else at -20°C .

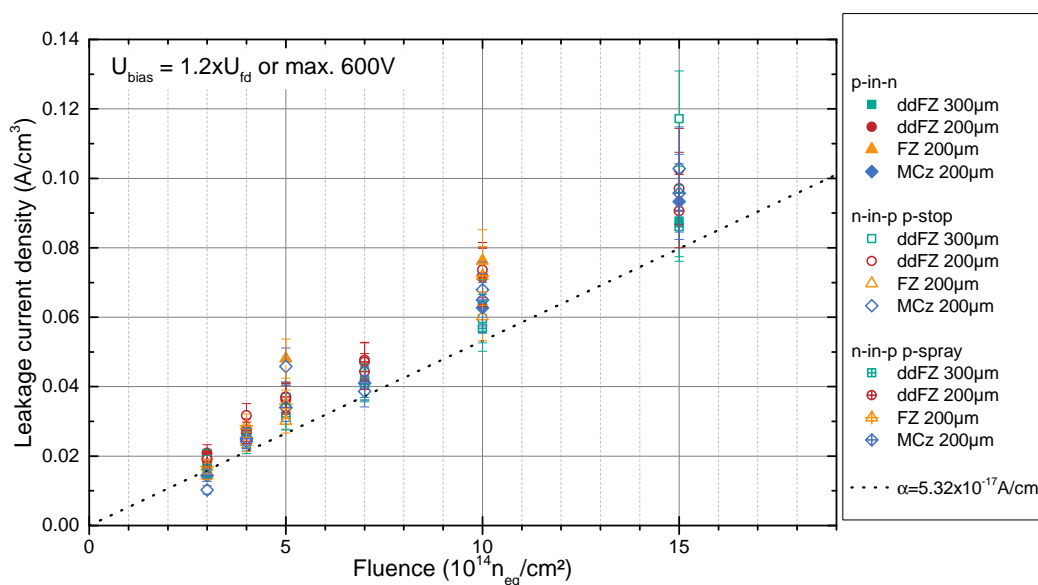
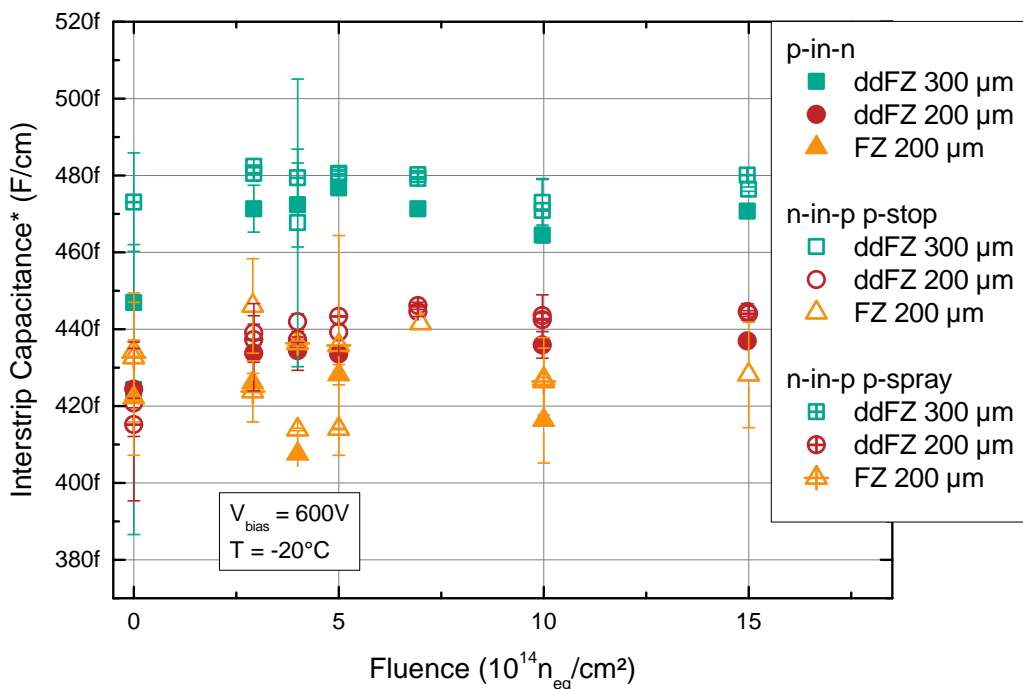


Figure 5. Leakage currents of strip sensors as extracted from IV measurements [32]. The dashed line indicates the expectation for diodes according to [27]. Measurements were performed at -20°C and at a bias voltage 20% above the full depletion voltage (but maximum 600 V). These currents reflect the expectation during operation conditions and are used to predict power consumption and heat load. These values are not meant to provide the material specific damage rate.



* to one neighboring strip @ 1MHz

Figure 6. Interstrip capacitance to one neighboring strip at a frequency of 1 MHz vs. irradiation fluence. The data points are mean values at 600 V with error bars representing the RMS for several strips (eventually also on several sensors). The systematic uncertainty is estimated to 5%.

clusters or disappearing signals. Therefore the p-stop concentration used must have as high a value as possible. This approach is also implemented in many sensor designs and works well for non-irradiated sensors. However, recent studies have shown [38, 39] that a peak concentration of the p-stop doping above $1 \times 10^{17} cm^{-3}$ might generate excessive electric fields at the p-stops after irradiation. This could lead to discharge or avalanche effects which degrade the performance.

4.2 Charge collection and noise

After the electrical characterization, the sensors were read out by the ALiBaVa system at $-20^\circ C$ using a Sr-90 source. The results of the charge collection measurements are summarized in figure 8 for sensors with a nominal active thickness of 300 μm . The faster decrease of the collected charge with fluence can be clearly seen for p-in-n type sensors compared to n-in-p type sensors, which is in line with results from RD50,³ e.g. [40]. With increasing fluence, trapping effects [41, 42] become more and more dominant and hole collection (at p-type strips) is a clear disadvantage due to the much lower mobility and therefore longer drift time of the holes. In figure 8 a lower seed signal is observed for n-in-p type sensors at the first irradiation step of $3 \times 10^{14} n_{eq}/cm^2$, which is due to wider clusters in those sensors resulting in a smaller seed signal. This difference can originate from

³Radiation hard semiconductor devices for very high luminosity colliders, <http://rd50.web.cern.ch/rd50/>

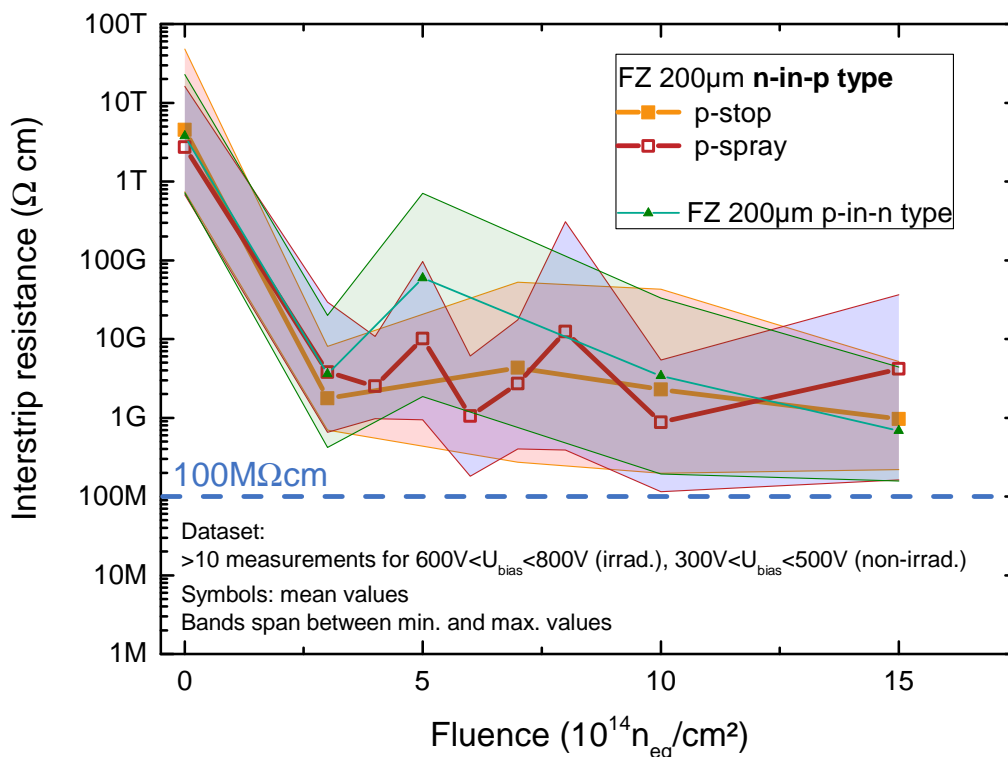


Figure 7. Interstrip resistance to the neighboring strip vs. irradiation fluence for nominal 200 μm thick sensors. The resistance is normalized to 1 cm strip length. Each data point indicates the mean of at least ten measurements (different strips on same sensor) on fully depleted sensors. The bands indicate the maximum and minimum values measured. Measurements on non-irradiated samples were performed at room temperature, else at -20°C .

the positive oxide charge generated by ionizing radiation [8, 10] leading to an electron accumulation in the n-in-p type sensors and a resulting alteration of the electric fields close to the strips [43]. The total cluster signal is similar to (or in this example even exceeds) the one from p-in-n type sensors at this fluence as indicated by the open symbols in figure 8.

Looking at the charge collection of sensors with a nominal active thickness of 200 μm (figure 9) the difference of collecting electrons versus holes is not visible due to the higher electric field at the same bias voltage of 600 V. The plot also shows the seed signals of three different particle types at the fluence point $1 \times 10^{15} \text{ n}_{\text{eq}}/\text{cm}^2$, which are very closely spread around 9000 e^- and demonstrate that the particle type does not change the results significantly. Also in figure 9 one can see the difference of measured cluster charge (open symbols) versus seed charge after an irradiation fluence of $3 \times 10^{14} \text{ n}_{\text{eq}}/\text{cm}^2$ for 200 μm . One could conclude from the seed signals in figure 9 that p-in-n sensors are compatible or slightly superior to n-in-p. This assessment changes when looking at the noise performance. For irradiated p-in-n sensors with a nominal active thickness of 200 μm a strong non-Gaussian noise component on all strips was observed, which cannot be suppressed by hit reconstruction algorithms and thus produces misidentified hits [44]. Examples

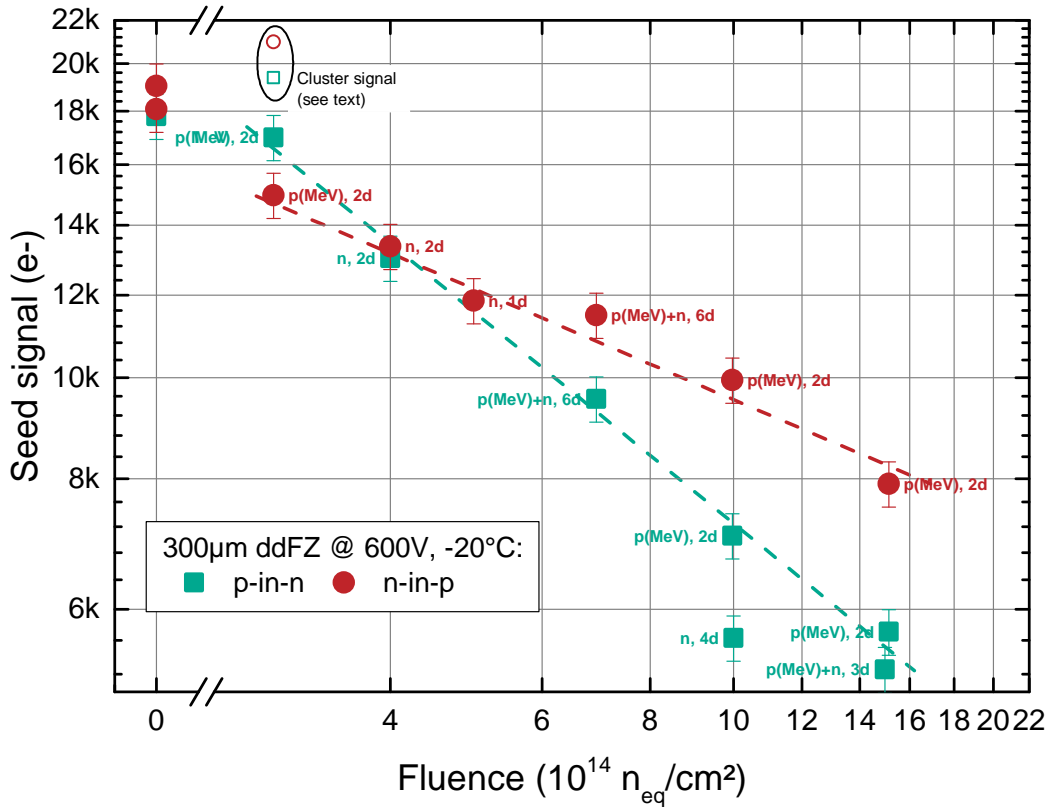


Figure 8. Charge collected on the seed strip for sensors of a nominal active thickness of $300\mu\text{m}$ after a short annealing time of between 2 and 6 days at room temperature. The error bars reflect an estimated uncertainty of about 5% representing statistical and gain uncertainties. The text next to the symbols indicates the irradiation type (**p** stands for protons with energy range MeV/GeV and **n** for neutrons) and the equivalent annealing time at 21°C . The lines should guide the eye.

of noise distributions with and without the non-Gaussian component are shown in figure 10, for which the average over all events per channel (pedestal) was subtracted from the raw data. It is obvious that applying a threshold of 5σ of the Gaussian fit does not eliminate misidentified hits due to the long noise tails. To quantify this effect a 5σ threshold was applied to these distributions and the misidentification occupancy was calculated by summing up all entries above this threshold and dividing by the number of events and the number of active read-out strips. Figure 11 shows several plots of this quantity as a function of bias voltage and equivalent annealing time at room temperature.⁴ A significantly large area (red) represents operation conditions under which the sensors show a misidentified hit occupancy above 1%. This value is considered severe since one expects an occupancy of real particle hits of the same amount in the future outer tracker. These misidentified hits are already observed at a proton fluence of $3 \times 10^{14} n_{eq}/\text{cm}^2$. The occupancy

⁴Annealing is performed at elevated temperatures and the acceleration factor of the current annealing from [27] was applied.

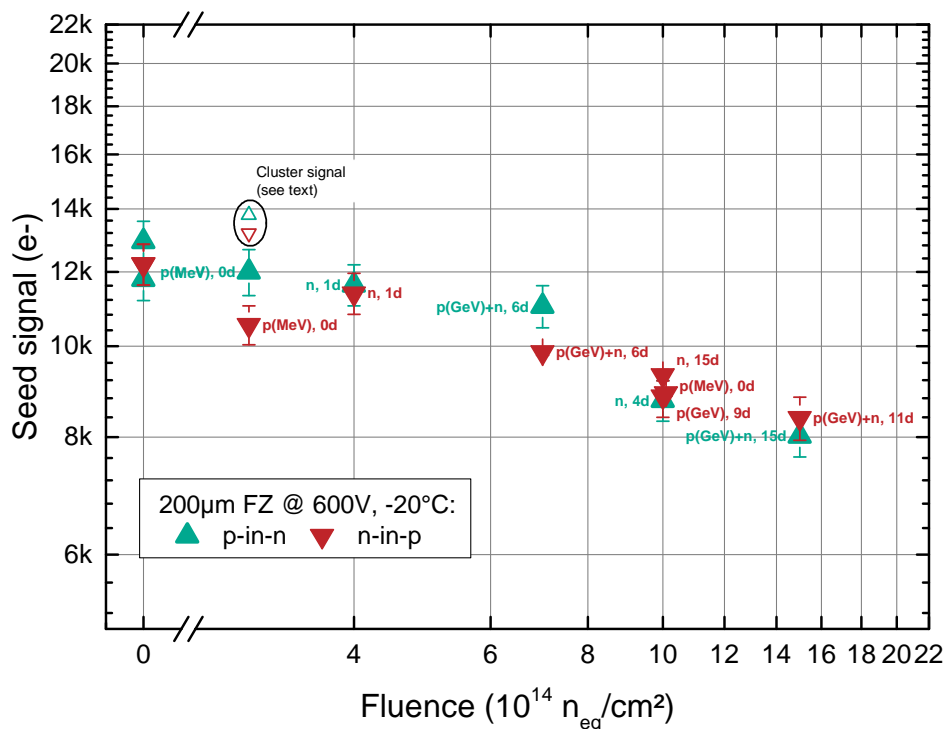


Figure 9. Charge collected on the seed strip for sensors with a nominal active thickness of 200 μm after a short annealing time of between 0 and 15 days at room temperature. The error bars reflect an estimated uncertainty of about 5% representing statistical and gain uncertainties. The text next to the symbols indicates the irradiation type (**p** stands for protons with energy range MeV/GeV and **n** for neutrons) and the equivalent annealing time at 21 $^{\circ}\text{C}$.

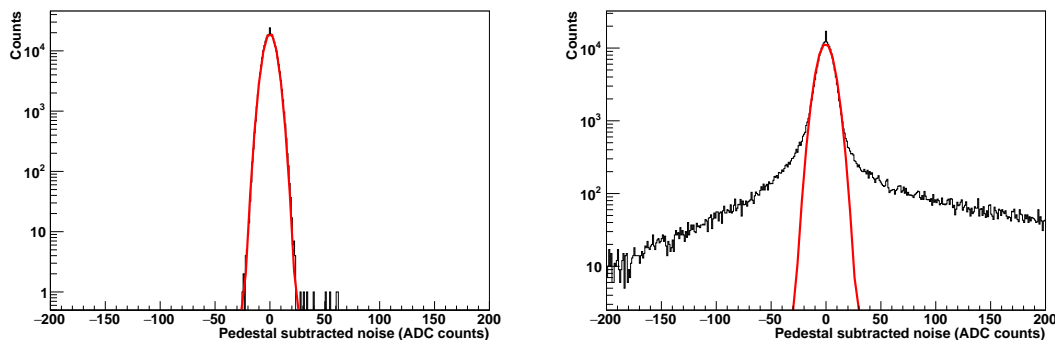


Figure 10. Two examples of pedestal-subtracted noise distributions as measured with the ALiBaVa system and fitted by a Gaussian distribution: a normal noise distribution (left) as observed on p-in-n type FZ sensors before irradiation, which looks similar for n-in-p sensors (both non-irradiated and irradiated), and a noise distribution affected by the non-Gaussian component observed for irradiated p-in-n FZ sensors with a nominal active thickness of 200 μm (right).

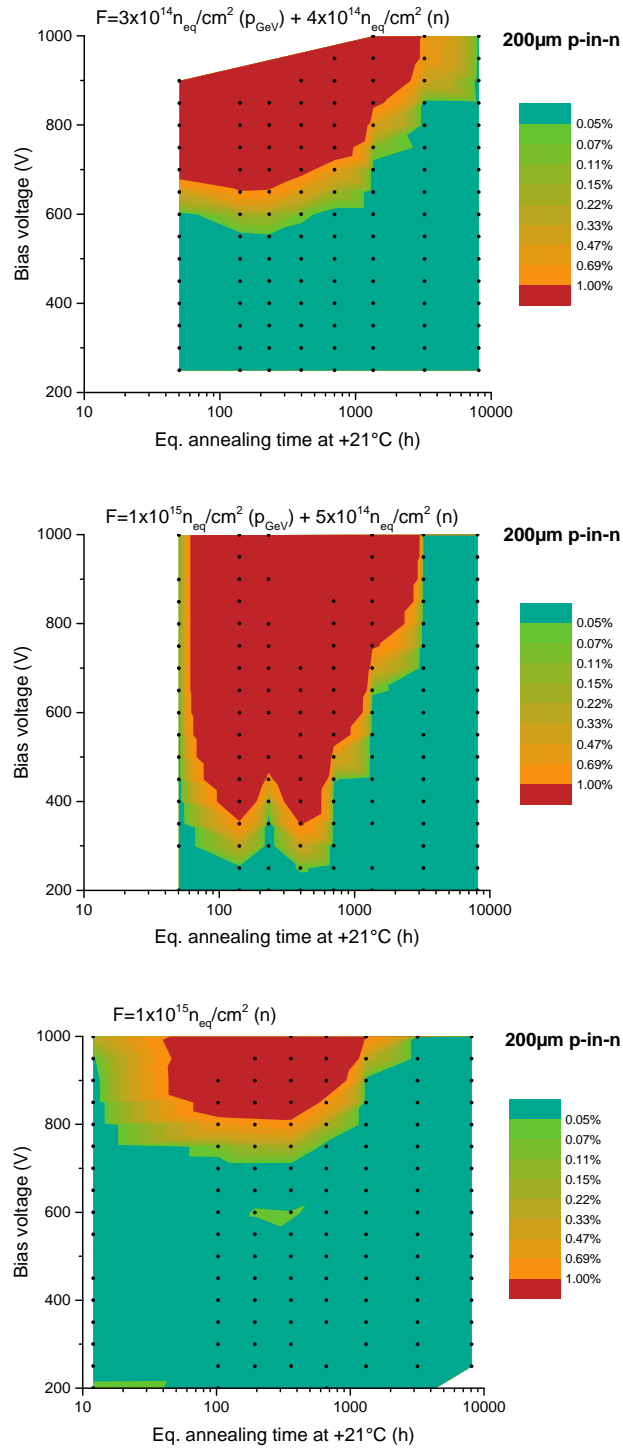


Figure 11. Measured occupancy of misidentified hits generated by non-Gaussian noise. These examples are for p-in-n sensors with 200µm active and physical thickness irradiated to $7 \times 10^{14} n_{eq}/cm^2$ (top) and $1.5 \times 10^{15} n_{eq}/cm^2$ (center) with mixed particles and to $1 \times 10^{15} n_{eq}/cm^2$ with only neutrons (bottom). The black dots represent the data points and the color code interpolates between them. White areas lie outside the measurement range.

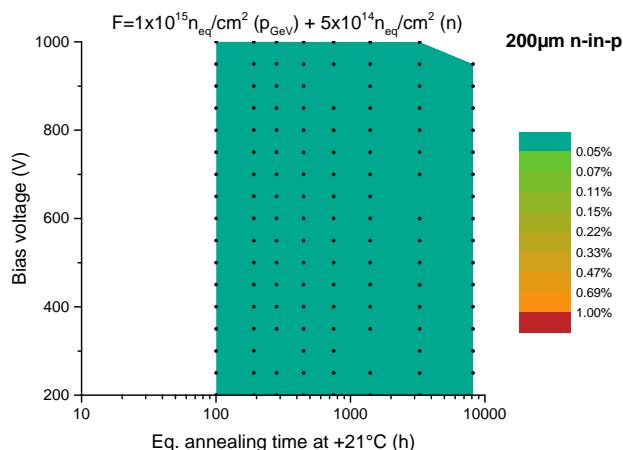


Figure 12. Measured occupancy of misidentified hits generated by non-Gaussian noise. This example is for an n-in-p type sensor with a nominal active and physical thickness of 200 μm irradiated to $1.5 \times 10^{15} \text{ n}_{\text{eq}}/\text{cm}^2$ mixed fluence.

increases with temperature and it strongly depends on the applied bias voltage, which suggests that the non-Gaussian noise originates from high electric fields. This coincides with the finding that thin sensors with a higher maximum electric field at the same bias voltage are more affected. In addition, it was observed that p-in-n sensors irradiated only with neutrons also show misidentified hits but at higher bias voltages (figure 11 (bottom)).

Non-Gaussian noise was not observed in n-in-p type sensors as can be seen from figure 12. To reproduce and understand this effect, TCAD simulations were performed. These simulations are discussed in the next section.

5 Simulation of electric fields

For the device simulations, the commercial TCAD software packages from Synopsys [46] and Silvaco [47] were used. Effective defect models were developed in [38, 48] for proton and neutron irradiated sensors. The defect properties of the model in Synopsys tuned to data from proton irradiated samples are listed in table 3. The electric field in the region between two strips of a 200 μm thick strip sensor was simulated at a bias voltage of 1000 V (higher bias voltage than nominal operation voltage of 600 V to enhance high field effects; qualitative differences are not expected) with bulk defect concentrations corresponding to a fluence of $1 \times 10^{15} \text{ n}_{\text{eq}}/\text{cm}^2$ for a p-in-n and an n-in-p configuration. The surface damage was introduced by increasing the fixed oxide charge at the Si-SiO₂ interface. The electric field strength at 1.3 μm below the Si-SiO₂ interface (approximate depth of the strip doping profile) is plotted in figure 13 for the two different configurations. The two plots show that the maximum electric field is always at the strip edge for both configurations and that for p-in-n type sensors the electric field increases with increasing oxide charge (N_{ox}), while it decreases for n-in-p type sensors. Such an increase in oxide charge (fast increase and saturation around $2 \times 10^{12} \text{ cm}^{-2}$ at 10 kGy [7, 8]) is expected due to the ionizing radiation in the detector and therefore only the red lines with high N_{ox} should be considered for

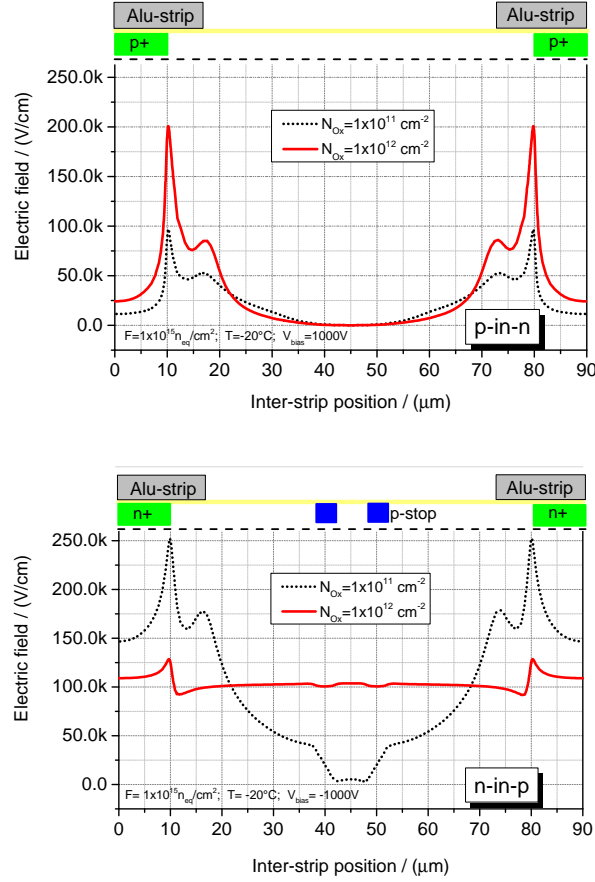


Figure 13. Simulated electric field strength 1.3 μm below the Si-SiO₂ interface after bulk damage equivalent to $1 \times 10^{15} \text{ n}_{\text{eq}}/\text{cm}^2$ at 1000 V bias voltage and a temperature of -20°C . N_{ox} of $1 \times 10^{11} \text{ cm}^{-2}$ and $1 \times 10^{12} \text{ cm}^{-2}$ correspond approximately to a total ionizing dose of 10 Gy and 10 kGy, respectively. The upper part of the plot includes a sketch of the surface layout. The upper plot represents a p-in-n type sensor and the lower plot an n-in-p type sensor [49]. The simulations were performed with Synopsys TCAD.

Table 3. Properties of the two bulk defects used for the simulations. E_V and E_C are the energies of the valence and conduction band, respectively, while $\sigma(e)$ and $\sigma(h)$ are the cross sections for electrons and holes and F stands for the fluence [48].

Parameter	Defect 1	Defect 2
Type	Donor	Acceptor
Energy (eV)	$E_V + 0.48$	$E_C - 0.525$
Concentration (cm^{-3})	$5.598 \text{ cm}^{-1} \times F - 3.949 \cdot 10^{14}$	$1.189 \text{ cm}^{-1} \times F - 6.454 \cdot 10^{13}$
$\sigma(e)$ (cm^2)	$1.0 \cdot 10^{-14}$	$1.0 \cdot 10^{-14}$
$\sigma(h)$ (cm^2)	$1.0 \cdot 10^{-14}$	$1.0 \cdot 10^{-14}$

the validation at the expected radiation conditions. Similar simulations were carried out using Silvaco and a slightly modified defect model resulting in the same conclusion being drawn [38, 45]. The outcome of the simulations could explain the tails observed in the pedestal-subtracted noise distributions of figure 10 for p-in-n type sensors: thermally generated charge carriers could be accelerated in the high electric field regions found in the simulations and be subject to an avalanche type multiplication generating a random signal.

The simulation results confirm that after radiation exposure to the expected doses for HL-LHC, sensors with the n-in-p type configuration are a more robust choice for the CMS Tracker application. Since this qualitative result is obtained with a 2D simulation taking into account only a slice of 1 μm it is valid for long strips as well as shorter macro-pixel sensors. The small potential difference on the implanted strips of AC and DC coupled sensors is not expected to change the conclusion. While an adaptation of the design could lead to robust p-in-n sensors, as shown in [50, 51], this was not investigated by the collaboration.

6 Conclusion

A variety of different silicon base materials and technologies were investigated using sensors and test structures produced by a single manufacturer. Miniature strip sensors were characterized before and after irradiations up to the levels expected for the HL-LHC operation period. The characterizations included electrical measurements of the sensor parameters, charge collection, noise occupancy measurements and annealing studies.

Comparing the performance of the sensors the collaboration has concluded that n-in-p type sensors are the most appropriate choice for operation in the CMS outer tracker region at HL-LHC. The main considerations were:

- It was confirmed that strip isolation of n-in-p sensors can be well controlled using either p-stop or p-spray technology.
- Sensors with n-type readout strips mainly collecting electrons provide equivalent or higher signals after irradiations beyond $5 \times 10^{14} \text{ n}_{\text{eq}}/\text{cm}^2$ than achieved for p-in-n sensors for equal thickness and bias voltage.
- The investigated p-in-n type sensors show non-Gaussian noise effects after irradiation related to high electric fields, while n-in-p type sensors do not.
- Compared to n-in-n type sensors, the n-in-p process is single-sided and presumably available at lower costs. Also the n-in-p sensors are less sensitive to scratches on the back side.

Acknowledgments

The research leading to these results has received funding from the European Commission under the FP7 Research Infrastructures project AIDA, Grant agreement no. 262025.

References

- [1] <http://hilumilhc.web.cern.ch/about/hl-lhc-project>.
- [2] I. Bejar Alonso, L. Rossi, *HiLumi LHC Technical Design Report*, CERN-ACC-2015-0140 (2015).
- [3] D. Contardo et al., *Technical Proposal for the Phase-II Upgrade of the CMS Detector*, CERN-LHCC-2015-010.
- [4] CMS collaboration, *The CMS Experiment at the CERN LHC*, 2008 JINST 3 S08004.
- [5] CMS collaboration, *1-D plot covering CMS tracker, showing FLUKA simulated 1 MeV neutron equivalent in Silicon including contributions from various particle types.*, CMS-DP-2015-022.
- [6] M. Huhtinen, *Simulation of non-ionising energy loss and defect formation in silicon*, *Nucl. Instrum. Meth. A* 491 (2002) 194.
- [7] J. Zhang, *X-ray Radiation Damage Studies and Design of a Silicon Pixel Sensor for Science at the XFEL*, DESY (2013) [DESY-THESIS-13-018].
- [8] J. Zhang et al., *Study of radiation damage induced by 12 keV X-rays in MOS structures built on high-resistivity n-type silicon*, *J. Synchrotron Rad.* 19 (2012) 340.
- [9] T.P. Ma and P. Dressendorfer, *Ionizing Radiation Effects in MOS Devices and Circuits*, Wiley (1989) [ISBN: 978-0-471-84893-6].
- [10] T.R. Oldham and F.B. McLean, *Total ionizing dose effects in MOS oxides and devices*, *IEEE Trans. Nucl. Sci.* 50 (2003) 483.
- [11] K.H. Hoffmann, *Campaign to identify the future CMS tracker baseline*, *Nucl. Instrum. Meth. A* 658 (2011) 30.
- [12] G. Auzinger, *Silicon sensor development for the CMS tracker upgrade*, 2011 JINST 6 P10010.
- [13] G. Steinbrück on behalf of the CMS Tracker collaboration, *Towards radiation hard sensor materials for the CMS tracker upgrade*, in proceedings of *IEEE Nuclear Science Symposium and Medical Imaging Conference (NSS/MIC)*, 2012, pp. 1828–1832.
- [14] A. Dierlamm, *Characterisation of silicon sensor materials and designs for the CMS Tracker Upgrade*, PoS(VERTEX 2012)016.
- [15] D. Eckstein, *CMS outer tracker upgrade plans*, PoS(VERTEX2013)015.
- [16] B. Lutzer, *Characterization of irradiated test structures for the CMS tracker upgrade*, *Nucl. Instrum. Meth. A* 730 (2013) 204.
- [17] G. Auzinger, *Analysis of testbeam data of irradiated silicon prototype sensors for the CMS tracker upgrade*, *Nucl. Instrum. Meth. A* 730 (2013) 195.
- [18] A. Junkes, *Planar silicon sensors for the CMS tracker upgrade*, *Nucl. Instrum. Meth. A* 732 (2013) 113.
- [19] A. Nürnberg and T. Schneider, *Lorentz angle measurements as part of the sensor R&D for the CMS Tracker upgrade*, 2013 JINST 8 C01001.
- [20] M. Bernard-Schwarz, *Future silicon sensors for the CMS Tracker upgrade*, *Nucl. Instrum. Meth. A* 699 (2013) 89.
- [21] CMS TRACKER collaboration, M. Printz, *Radiation hard sensor materials for the CMS Tracker Phase II Upgrade - Charge collection of different bulk polarities*, *Nucl. Instrum. Meth. A* 765 (2014) 29.

- [22] G. Lutz, *Semiconductor Radiation Detectors — Device Physics*, Springer (1999) [ISBN 3-540-64859-3].
- [23] A. Junkes, *Influence of radiation induced defect clusters on silicon particle detectors*, Ph.D. thesis, University of Hamburg (2011) [DESY-THESIS-2011-031].
- [24] CMS collaboration, *The CMS tracker system project: Technical Design Report*, CERN-LHCC-98-006 (1997).
- [25] CMS collaboration, *The CMS tracker: addendum to the Technical Design Report*, CERN-LHCC-2000-016 (2000).
- [26] M. Huhtinen, *The radiation environment at the CMS experiment at the LHC*, Ph.D. thesis, Helsinki U. Tech. (1996) [HU-SEFT-R-1996-14].
- [27] M. Moll, *Radiation Damage in Silicon Particle Detectors*, Ph.D. thesis, University of Hamburg (1999), [DESY-THESIS-1999-040].
- [28] L. Snoj, G. Žerovnik and A. Trkov, *Computational analysis of irradiation facilities at the JSI TRIGA reactor*, *Appl. Radiat. Isotopes* **70** (2012) 483.
- [29] D. Zontar, V. Cindro, G. Kramberger and M. Mikuz, *Time development and flux dependence of neutron-irradiation induced defects in silicon pad detectors*, *Nucl. Instrum. Meth. A* **426** (1999) 51.
- [30] <https://ps-irrad.web.cern.ch/>.
- [31] http://www.ekp.kit.edu/english/irradiation_center.php.
- [32] K.-H. Hoffmann, *Development of new Sensor Designs and Investigations on Radiation Hard Silicon Strip Sensors for the CMS Tracker Upgrade at the High Luminosity Large Hadron Collider*, Ph.D. thesis, Karlsruhe Institute of Technology (2013) [IEKP-KA/2013-1].
- [33] R. Marco-Hernandez, *A portable readout system for silicon microstrip sensors*, *Nucl. Instrum. Meth. A* **623** (2010) 207, <http://www.alibavasystems.com>.
- [34] *The Beetle Reference Manual for Beetle version 1.3 / 1.4 / 1.5*, LHCb-2005-105, http://www.kip.uni-heidelberg.de/lhcb/Publications/BeetleRefMan_v1_3.pdf.
- [35] S. Löchner, *Development, Optimisation and Characterisation of a Radiation Hard Mixed-Signal Readout Chip for LHCb*, Ph.D. thesis, Combined Faculties for the Natural Sciences and for Mathematics of the Ruperto-Carola University of Heidelberg, Germany (2006) [<http://archiv.ub.uni-heidelberg.de/volltextserver/6708/>].
- [36] G. Hall et al., *CBC2: A CMS microstrip readout ASIC with logic for track-trigger modules at HL-LHC*, *Nucl. Instrum. Meth. A* **765** (2014) 214.
- [37] H. Bichsel, *Straggling in Thin Silicon Detectors*, *Rev. Mod. Phys.* **60** (1988) 663.
- [38] R. Dalal, A. Bhardwaj, K. Ranjan, M. Moll and A. Elliott-Peisert, *Combined effect of bulk and surface damage on strip insulation properties of proton irradiated n^+ -p silicon strip sensors*, 2014 *JINST* **9** P04007.
- [39] M. Printz, *P-stop isolation study of irradiated n-in-p type silicon strip sensors for harsh radiation environments*, *Nucl. Instrum. Meth. A* **831** (2016) 38.
- [40] A. Affolder, P. Allport and G. Casse, *Collected charge of planar silicon detectors after pion and proton irradiations up to $2.2 \times 10^{16} n_{eq} cm^{-2}$* , *Nucl. Instrum. Meth. A* **623** (2010) 177.
- [41] CMS TRACKER GROUP collaboration, *Trapping in proton irradiated p^+ -n- n^+ silicon sensors at fluences anticipated at the HL-LHC outer tracker*, 2016 *JINST* **11** P04023 [arXiv:1505.01824].

- [42] G. Kramberger, V. Cindro, I. Mandic, M. Mikuz and M. Zavrtanik, *Effective trapping time of electrons and holes in different silicon materials irradiated with neutrons, protons and pions*, *Nucl. Instrum. Meth. A* **481** (2002) 297.
- [43] CMS TRACKER GROUP collaboration, *Impact of low-dose electron irradiation on n^+p silicon strip sensors*, *Nucl. Instrum. Meth. A* **803** (2015) 100 [[arXiv:1505.02672](https://arxiv.org/abs/1505.02672)].
- [44] A. Dierlamm, *Planar sensors for future Vertex and Tracking Detectors*, *PoS(VERTEX2013)*027.
- [45] R. Dalal, *Simulation of Irradiated Detectors*, *PoS(VERTEX2014)*030.
- [46] <https://www.synopsys.com/silicon/tcad.html>.
- [47] Silvaco Inc., *Atlas Users Manual*, <https://dynamic.silvaco.com/dynamicweb/jsp/downloads/DownloadManualsAction.do?req=silen-manuals&nm=atlas>.
- [48] R. Eber, *Investigations of new Sensor Designs and Development of an effective Radiation Damage Model for the Simulation of highly irradiated Silicon Particle Detectors*, Ph.D. thesis, Karlsruhe Institute of Technology (2013), [[IEKP-KA/2013-27](https://arxiv.org/abs/1303.2727)].
- [49] M. Printz, *T-CAD analysis of electric fields in n-in-p silicon strip detectors in dependence on the p-stop pattern and doping concentration*, 2015 *JINST* **10** C01048.
- [50] J. Schwandt, E. Fretwurst, R. Klanner, I. Kopsalis and J. Zhang, *Design and First Tests of a Radiation-Hard Pixel Sensor for the European X-Ray Free-Electron Laser*, *IEEE Trans. Nucl. Sci.* **61** (2014) 1894 [[arXiv:1402.3129](https://arxiv.org/abs/1402.3129)].
- [51] J. Schwandt, *Design of a Radiation Hard Silicon Pixel Sensor for X-ray Science*, Ph.D. thesis, University of Hamburg (2014) [DESY-THESIS-2014-029].

Tracker group of the CMS collaboration

Institut für Hochenergiephysik, Wien, Austria

W. Adam, T. Bergauer, E. Brondolin, M. Dragicevic, M. Friedl, R. Frühwirth,¹ M. Hoch, J. Hrubec, A. König, H. Steininger, W. Waltenberger

Universiteit Antwerpen, Antwerpen, Belgium

S. Alderweireldt, W. Beaumont, X. Janssen, J. Lauwers, P. Van Mechelen, N. Van Remortel, A. Van Spilbeeck

Université Libre de Bruxelles, Bruxelles, Belgium

D. Beghin, H. Brun, B. Clerbaux, H. Delannoy, G. De Lentdecker, G. Fasanella, L. Favart, R. Goldouzian, A. Grebenyuk, G. Karapostoli, Th. Lenzi, A. Léonard, J. Luetic, N. Postiau, T. Seva, P. Vanlaer, D. Vannerom, Q. Wang, F. Zhang

Vrije Universiteit Brussel, Brussel, Belgium

S. Abu Zeid, F. Blekman, I. De Bruyn, J. De Clercq, J. D'Hondt, K. Deroover, S. Lowette, S. Moortgat, L. Moreels, Q. Python, K. Skovpen, P. Van Mulders, I. Van Parijs

Université Catholique de Louvain, Louvain-la-Neuve, Belgium

H. Bakhshiansohi, O. Bondu, S. Brochet, G. Bruno, A. Caudron, C. Delaere, M. Delcourt, S. De Visscher, B. Francois, A. Giammanco, A. Jafari, M. Komm, G. Krintiras, V. Lemaitre, A. Magitteri, A. Mertens, D. Michotte, M. Musich, K. Piotrkowski, L. Quertenmont, N. Szilasi, M. Vidal Marono, S. Wertz

Université de Mons, Mons, Belgium

N. Belyi, T. Caebergs, E. Daubie, G.H. Hammad

Helsinki Institute of Physics, Helsinki, Finland

J. Härkönen, T. Lampén, P. Luukka, T. Peltola, E. Tuominen, E. Tuovinen

Department of Physics, University of Helsinki, Helsinki, Finland

P. Eerola

Lappeenranta University of Technology, Lappeenranta, Finland

T. Tuuva

Université de Lyon, Université Claude Bernard Lyon 1, CNRS-IN2P3, Institut de Physique Nucléaire de Lyon, Villeurbanne, France

G. Baulieu, G. Boudoul, L. Caponetto, C. Combaret, D. Contardo, T. Dupasquier, G. Gallbit, N. Lumb, L. Mirabito, S. Perries, M. Vander Donckt, S. Viret

Université de Strasbourg, CNRS, IPHC UMR 7178, Strasbourg, France

J.-L. Agram,² J. Andrea, D. Bloch, C. Bonnin, J.-M. Brom, E. Chabert, N. Chanon, L. Charles, E. Conte,² J.-Ch. Fontaine,² L. Gross, J. Hosselet, M. Jansova, D. Tromson

RWTH Aachen University, I. Physikalisches Institut, Aachen, Germany

C. Autermann, L. Feld, W. Karpinski, K.M. Kiesel, K. Klein, M. Lipinski, A. Ostapchuk, G. Pierschel, M. Preuten, M. Rauch, S. Schael, C. Schomakers, J. Schulz, G. Schwering, M. Wlochal, V. Zhukov

RWTH Aachen University, III. Physikalisches Institut B, Aachen, Germany

C. Pistone, G. Fluegge, A. Kuensken, O. Pooth, A. Stahl

Deutsches Elektronen-Synchrotron, Hamburg, Germany

M. Aldaya, C. Asawatangtrakuldee, K. Beernaert, D. Bertsche, C. Contreras-Campana, G. Eckerlin, D. Eckstein, T. Eichhorn, E. Gallo, J. Garay Garcia, K. Hansen, M. Haranko, A. Harb, J. Hauk, J. Keaveney, A. Kalogeropoulos, C. Kleinwort, W. Lohmann,³ R. Mankel, H. Maser, G. Mittag, C. Muhl, A. Mussgiller, D. Pitzl, O. Reichelt, M. Savitskyi, P. Schuetze, R. Walsh, A. Zuber

University of Hamburg, Hamburg, Germany

H. Biskop, P. Buhmann, M. Centis-Vignali, E. Garutti, J. Haller, M. Hoffmann, T. Lapsien, M. Matysek, A. Perieanu, Ch. Scharf, P. Schleper, A. Schmidt, J. Schwandt, J. Sonneveld, G. Steinbrück, B. Vormwald, J. Wellhausen

Institut für Experimentelle Kernphysik, Karlsruhe, Germany

M. Abbas, C. Amstutz, T. Barvich, Ch. Barth, F. Boegelspacher, W. De Boer, E. Butz, M. Caselle, F. Colombo, A. Dierlamm, B. Freund, F. Hartmann, S. Heindl, U. Husemann, A. Kornmayer, S. Kudella, Th. Muller, H.J. Simonis, P. Steck, M. Weber, Th. Weiler

Institute of Nuclear and Particle Physics (INPP), NCSR Demokritos, Aghia Paraskevi, Greece

G. Anagnostou, P. Asenov, P. Assiouras, G. Daskalakis, A. Kyriakis, D. Loukas, L. Paspalaki

Wigner Research Centre for Physics, Budapest, Hungary

F. Siklér, V. Veszprémi

University of Delhi, Delhi, India

A. Bhardwaj, R. Dalal, G. Jain, K. Ranjan

Institute for Research in Fundamental Sciences (IPM), Tehran, Iran

H. Bakhshiansohl, H. Behnamian, M. Khakzad, M. Naseri

INFN Sezione di Bari,^a Università di Bari,^b Politecnico di Bari,^c Bari, Italy

P. Cariola,^a D. Creanza,^{a,c} M. De Palma,^{a,b} G. De Robertis,^a L. Fiore,^a M. Franco,^{a,b} F. Loddo,^a L. Silvestris,^a G. Maggi,^{a,c} S. Martiradonna,^a S. My,^{a,b} G. Selvaggi^{a,b}

INFN Sezione di Catania,^a Università di Catania,^b Catania, Italy

S. Albergo,^{a,b} G. Cappello,^{a,b} M. Chiorboli,^{a,b} S. Costa,^{a,b} A. Di Mattia,^a F. Giordano,^{a,b} R. Potenza,^{a,b} M.A. Saizu,^{a,4} A. Tricomi,^{a,b} C. Tuve^{a,b}

INFN Sezione di Firenze,^a Università di Firenze,^b Firenze, Italy

G. Barbagli,^a M. Brianzi,^a R. Ciaranfi,^a V. Ciulli,^{a,b} C. Civinini,^a R. D'Alessandro,^{a,b} E. Focardi,^{a,b} G. Latino,^{a,b} P. Lenzi,^{a,b} M. Meschini,^a S. Paoletti,^a L. Russo,^{a,b} E. Scarlini,^{a,b} G. Sguazzoni,^a D. Strom,^a L. Viliani^{a,b}

INFN Sezione di Genova,^a Università di Genova,^b Genova, Italy

F. Ferro,^a M. Lo Vetere,^{a,b} E. Robutti^a

INFN Sezione di Milano-Bicocca,^a Università di Milano-Bicocca,^b Milano, Italy

M.E. Dinardo,^{a,b} S. Fiorendi,^{a,b} S. Gennai,^a S. Malvezzi,^a R.A. Manzoni,^{a,b} D. Menasce,^a
L. Moroni,^a D. Pedrini^a

INFN Sezione di Padova,^a Università di Padova,^b Padova, Italy

P. Azzi,^a N. Bacchetta,^a D. Bisello,^a M. Dall'Osso,^{a,b} N. Pozzobon,^{a,b} M. Tosi^{a,b}

INFN Sezione di Pavia,^a Università di Bergamo,^b Italy

F. De Canio,^{a,b} L. Gaioni,^{a,b} M. Manghisoni,^{a,b} B. Nodari,^{a,b} E. Riceputi,^{a,b} V. Re,^{a,b}
G. Traversi^{a,b}

INFN Sezione di Pavia,^a Università di Pavia,^b Pavia, Italy

D. Comotti,^{a,b} L. Ratti^{a,b}

INFN Sezione di Perugia,^a Università di Perugia,^b Perugia, Italy

L. Alunni Solestizi,^{a,b} M. Biasini,^{a,b} G.M. Bilei,^a C. Cecchi,^{a,b} B. Checcucci,^a
D. Ciangottini,^{a,b} L. Fanò,^{a,b} C. Gentsos,^a M. Ionica,^a R. Leonardi,^{a,b} E. Manoni,^{a,b}
G. Mantovani,^{a,b} S. Marconi,^{a,b} V. Mariani,^{a,b} M. Menichelli,^a A. Modak,^{a,b} A. Morozzi,^{a,b}
F. Moscatelli,^a D. Passeri,^{a,b} P. Placidi,^{a,b} V. Postolache,^a A. Rossi,^{a,b} A. Saha,^a
A. Santocchia^{a,b} L. Storchi,^a D. Spiga^a

INFN Sezione di Pisa,^a Università di Pisa,^b Scuola Normale Superiore di Pisa,^c Pisa, Italy

K. Androsova,^{a,5} P. Azzurri,^a S. Arezzini,^a G. Bagliesi,^a A. Basti,^a T. Boccali,^a L. Borrello,^a
F. Bosi,^a R. Castaldi,^a A. Ciampa,^a M.A. Ciocci,^{a,6} R. Dell'Orso,^a S. Donato,^{a,c} G. Fedi,^a
A. Giassi,^a M.T. Grippo,^{a,6} F. Ligabue,^{a,c} T. Lomtadze,^a G. Magazzu,^a L. Martini,^{a,b}
E. Mazzoni,^a A. Messineo,^{a,b} A. Moggi,^a F. Morsani,^a F. Palla,^a F. Palmonari,^a F. Raffaelli,^a
A. Rizzi,^{a,b} A. Savoy-Navarro,^{a,7} P. Spagnolo,^a R. Tenchini,^a G. Tonelli,^{a,b} A. Venturi,^a
P.G. Verdini^a

INFN Sezione di Torino,^a Università di Torino,^b Torino, Italy

R. Bellan,^{a,b} M. Costa,^{a,b} R. Covarelli,^{a,b} M. Da Rocha Rolo,^a N. Demaria,^a A. Rivetti,^a
G. Dellacasa,^a G. Mazza,^a E. Migliore,^{a,b} E. Monteil,^{a,b} L. Pacher,^a F. Ravera,^{a,b} A. Solano^{a,b}

Instituto de Física de Cantabria (IFCA), CSIC-Universidad de Cantabria, Santander, Spain

M. Fernandez, G. Gomez, R. Jaramillo Echeverria, D. Moya, F.J. Gonzalez Sanchez, I. Vila,
A.L. Virto

CERN, European Organization for Nuclear Research, Geneva, Switzerland

D. Abbaneo, I. Ahmed, E. Albert, G. Auzinger, G. Berruti, G. Bianchi, G. Blanchot, J. Bonnaud,
A. Caratelli, D. Ceresa, J. Christiansen, K. Cichy, J. Daguin, A. D'Auria, S. Detraz, D. Deyrail,
O. Dondelewski, F. Faccio, N. Frank, T. Gadek, K. Gill, A. Honma, G. Hugo, L.M. Jara Casas,
J. Kaplon, A. Kornmayer, L. Kottelat, M. Kovacs, M. Krammer,¹ P. Lenoir, M. Mannelli,
A. Marchioro, S. Marconi, S. Mersi, S. Martina, S. Michelis, M. Moll, A. Onnela, S. Orfanelli,
S. Pavis, A. Peisert, J.-F. Perrot, P. Petagna, G. Petrucciani, H. Postema, P. Rose, P. Tropea,
J. Troska, A. Tsirou, F. Vasey, P. Vichoudis, B. Verlaat, L. Zwalinski

Institute for Particle Physics, ETH Zurich, Zurich, Switzerland

F. Bachmair, R. Becker, D. di Calafiori, B. Casal, P. Berger, L. Djambazov, M. Donega, C. Grab, D. Hits, J. Hoss, G. Kasieczka, W. Lustermann, B. Mangano, M. Marionneau, P. Martinez Ruiz del Arbol, M. Masciovecchio, M. Meinhard, L. Perozzi, U. Roeser, A. Starodumov,⁸ V. Tavoraro, R. Wallny, D. Zhu

Universität Zürich, Zurich, Switzerland

C. Amsler,⁹ K. Bösiger, L. Caminada, F. Canelli, V. Chiochia, A. de Cosa, C. Galloni, T. Hreus, B. Kilminster, C. Lange, R. Maier, J. Ngadiuba, D. Pinna, P. Robmann, S. Taroni, Y. Yang

Paul Scherrer Institut, Villigen, Switzerland

W. Bertl[†], K. Deiters, W. Erdmann, R. Horisberger, H.-C. Kaestli, D. Kotlinski, U. Langenegger, B. Meier, T. Rohe, S. Streuli

National Taiwan University (NTU), Taipei, Taiwan

P.-H. Chen, C. Dietz, U. Grundler, W.-S. Hou, R.-S. Lu, M. Moya

University of Bristol, Bristol, United Kingdom

D. Cussans, H. Flacher, J. Goldstein, M. Grimes, J. Jacob, S. Seif El Nasr-Storey

Brunel University, Uxbridge, United Kingdom

J. Cole, C. Hoad, P. Hobson, A. Morton, I.D. Reid

Imperial College, London, United Kingdom

G. Auzinger, R. Bainbridge, P. Dauncey, G. Hall, T. James, A.-M. Mangan, M. Pesaresi, D.M. Raymond, K. Uchida

Rutherford Appleton Laboratory, Didcot, United Kingdom

J.A. Coughlan, K. Harder, J. Ilic, I.R. Tomalin

Brown University, Providence, U.S.A.

A. Garabedian, U. Heintz, M. Narain, J. Nelson, S. Sagir, T. Speer, J. Swanson, D. Tersegno, J. Watson-Daniels

University of California, Davis, Davis, U.S.A.

M. Chertok, J. Conway, R. Conway, C. Flores, R. Lander, D. Pellett, F. Ricci-Tam, M. Squires, J. Thomson, R. Yohay

University of California, Riverside, Riverside, U.S.A.

K. Burt, J. Ellison, G. Hanson, M. Olmedo, W. Si, B.R. Yates

University of California, San Diego, La Jolla, U.S.A.

R. Gerosa, V. Sharma, A. Vartak, A. Yagil, G. Zevi Della Porta

University of California, Santa Barbara — Department of Physics, Santa Barbara, U.S.A.

V. Dutta, L. Gouskos, J. Incandela, S. Kyre, S. Mullin, A. Patterson, H. Qu, D. White

The Catholic University of America, Washington DC, U.S.A.

A. Dominguez, R. Bartek

University of Colorado Boulder, Boulder, U.S.A.

J.P. Cumalat, W.T. Ford, F. Jensen, A. Johnson, M. Krohn, S. Leontsinis, T. Mulholland, K. Stenson, S.R. Wagner

Fermi National Accelerator Laboratory, Batavia, U.S.A.

A. Apresyan, G. Bolla[†], K. Burkett, J.N. Butler, A. Canepa, H.W.K. Cheung, J. Chramowicz, D. Christian, W.E. Cooper, G. Deptuch, G. Derylo, C. Gingu, S. Grünendahl, S. Hasegawa, J. Hoff, J. Howell, M. Hrycyk, S. Jindariani, M. Johnson, F. Kahlid, C.M. Lei, R. Lipton, R. Lopes De Sá, T. Liu, S. Los, M. Matulik, P. Merkel, S. Nahn, A. Prosser, R. Rivera, B. Schneider, G. Sellberg, A. Shenai, L. Spiegel, N. Tran, L. Uplegger, E. Voirin

University of Illinois at Chicago (UIC), Chicago, U.S.A.

D.R. Berry, X. Chen, L. Ennesser, A. Evdokimov, O. Evdokimov, C.E. Gerber, D.J. Hofman, S. Makauda, C. Mills, I.D. Sandoval Gonzalez

The Ohio State University, Columbus, U.S.A.

J. Alimena, L.J. Antonelli, B. Francis, A. Hart, C.S. Hill

Purdue University Calumet, Hammond, U.S.A.

N. Parashar, J. Stupak

Purdue University, West Lafayette, U.S.A.

D. Bortoletto, M. Bubna, N. Hinton, M. Jones, D.H. Miller, X. Shi

The University of Iowa, Iowa City, U.S.A.

P. Tan

The University of Kansas, Lawrence, U.S.A.

P. Baringer, A. Bean, S. Khalil, A. Kropivnitskaya, D. Majumder, G. Wilson

Kansas State University, Manhattan, U.S.A.

A. Ivanov, R. Mendis, T. Mitchell, N. Skhirtladze, R. Taylor

Johns Hopkins University, Baltimore, U.S.A.

I. Anderson, D. Fehling, A. Gritsan, P. Maksimovic, C. Martin, K. Nash, M. Osherson, M. Swartz, M. Xiao

University of Mississippi, Oxford, U.S.A.

J.G. Acosta, L.M. Cremaldi, S. Oliveros, L. Perera, D. Summers

University of Nebraska-Lincoln, Lincoln, U.S.A.

K. Bloom, D.R. Claes, C. Fangmeier, R. Gonzalez Suarez, J. Monroy, J. Siado

Northwestern University, Evanston, U.S.A.

K. Hahn, S. Sevova, K. Sung, M. Trovato

Rutgers, The State University of New Jersey, Piscataway, U.S.A.

E. Bartz, Y. Gershtein, E. Halkiadakis, S. Kyriacou, A. Lath, K. Nash, M. Osherson, S. Schnetzer, R. Stone, M. Walker

University of Puerto Rico, Mayaguez, U.S.A.

S. Malik, S. Norberg, J.E. Ramirez Vargas

State University of New York at Buffalo, Buffalo, U.S.A.

M. Alyari, J. Dolen, A. Godshalk, C. Harrington, I. Iashvili, A. Kharchilava, D. Nguyen,
A. Parker, S. Rappoccio, B. Roozbahani

Cornell University, Ithaca, U.S.A.

J. Alexander, J. Chaves, J. Chu, S. Dittmer, K. McDermott, N. Mirman, A. Rinkevicius, A. Ryd,
E. Salvati, L. Skinnari, L. Soffi, Z. Tao, J. Thom, J. Tucker, M. Zientek

Rice University, Houston, U.S.A.

B. Akgün, K.M. Ecklund, M. Kilpatrick, T. Nussbaum, J. Zabel

University of Rochester, Rochester, U.S.A.

B. Betchart, R. Covarelli, R. Demina, O. Hindrichs, G. Petrillo

Texas A&M University, College Station, U.S.A.

R. Eusebi, I. Osipenkov, A. Perloff, K.A. Ulmer

Vanderbilt University, Nashville, U.S.A.

A.G. Delannoy, P. D'Angelo, W. Johns

†: Deceased

1: Also at Vienna University of Technology, Vienna, Austria

2: Also at Université de Haute-Alsace, Mulhouse, France

3: Also at Brandenburg University of Technology, Cottbus, Germany

4: Also at Horia Hulubei National Institute of Physics and Nuclear Engineering (IFIN-HH), Bucharest,
Romania

5: Also at Università degli Studi di Siena, Siena, Italy

6: Also at Institut für Hochenergiephysik der OeAW, Wien, Austria

7: Also at CNRS-IN2P3, Paris, France

8: Also at Institute for Theoretical and Experimental Physics, Moscow, Russia

9: Also at Albert Einstein Center for Fundamental Physics, Bern, Switzerland